Acta Crystallographica Section B
Structural Science
ISSN 0108-7681

X-ray powder diffraction structural characterization of $Pb_{1-x}Ba_xZr_{0.65}Ti_{0.35}O_3$ ceramic

M. Mir,[a]* V. R. Mastelaro,[a] P. P. Neves,[a] A. C. Doriguetto,[b] D. Garcia,[c] M. H. Lente,[c] J. A. Eiras[c] and Y. P. Mascarenhas[a]

[a]Instituto de Fisica de Sao Carlos, Universidade de Sao Paulo, Caixa Postal 369, CEP 13560-970, Sao Carlos, SP Brasil, [b]Departamento de Ciencias Exatas – UNIFAL-MG, Rua Gabriel Monteiro da Silva 714, CEP 37130-000, Alfenas, MG Brasil, and [c]Departamento de Fisica, Universidade Federal de Sao Carlos, CEP 13565-905, Sao Carlos, SP, Brasil

Correspondence e-mail: mmir@ifsc.usp.br

Received 21 April 2006
Accepted 4 May 2007

The structure of $Pb_{1-x}Ba_xZr_{0.65}Ti_{0.35}O_3$ (PBZT) ceramic materials with $0.00 \leq x \leq 0.40$ was studied using synchrotron X-ray powder diffraction data. According to the Rietveld refinements, the structure of PBZT ceramics with $x = 0.00$, 0.10 and 0.20 at room temperature was rhombohedral *R*3*c*. A phase transition from rhombohedral to cubic was observed at 543 and 463 K for $x = 0.10$ and 0.20, respectively. The refinement for the compositions $x = 0.30$ and $x = 0.40$ showed a cubic structure from 10 to 450 K, in good agreement with the dielectric properties of these samples.

1. Introduction

$Pb(Zr_xTi_{1-x})O_3$ (commonly abbreviated as PZT) ceramics are used in a wide variety of piezoelectric, pyroelectric and ferroelectric memory devices (Jaffe *et al.*, 1971; Lines & Glass, 2001). Owing to their scientific and technological importance, structural details of PZT ceramics have been intensively investigated in recent years (Corker *et al.*, 1998; Noheda *et al.*, 1999; Ragini *et al.*, 2002; Frantti *et al.*, 2002; Joseph *et al.*, 2000; Woodward *et al.*, 2005; Kozielski *et al.*, 2006). These studies have been focused mainly on a morphotropic phase boundary which exists around the x = 0.45–0.50 compositions and presents special physical properties. According to the proposed phase diagram (Jaffe *et al.*, 1971), at the titanium-rich side of the phase diagram all compositions are tetragonal with *P*4*mm* symmetry. On the other hand (depending on x and temperature), two rhombohedral phases, *R*3*m* [often referred to as FR(HT)] and *R*3*c* [referred to as FR(LT)] are known to occur in Zr-rich PZT ceramics (Frantti *et al.*, 2002). The essential difference between the *R*3*m* and *R*3*c* phases is that the cell parameter c is doubled in the transition from *R*3*m* to *R*3*c* (Corker *et al.*, 1998). It has been shown that it is very difficult to differentiate the *R*3*m* and *R*3*c* phases by X-ray techniques because (although the *R*3*c* X-ray diffraction pattern exhibits all the systematic extinctions required by this space group) some of the very weak superlattice reflections could not be observed. In fact, these reflections were noticed when neutron powder diffraction was used but were not with X-rays, probably due to the small scattering factor of oxygen relative to the heavy atoms and poor discrimination from the background (Frantti *et al.*, 2002). Depending on the composition, cation shifts, octahedral tilts and deformations, other structures may occur. Therefore, the PZT phase diagram is rich and complex (Frantti *et al.*, 2002; Corker *et al.*, 1998).

In order to produce ceramic samples of technological interest at the Zr-rich side of the PZT phase diagram, metal ions such as lanthanum and barium have been added into PZT, including the composition with a Zr/Ti ratio equal to 65/35.

Table 1
The nominal and experimental compositions determined from ICP-AES measurements.

Sample	Nominal composition	Experimental composition
PBZT00	$PbZr_{0.65}Ti_{0.35}O_3$	$Pb_{0.98(2)}Zr_{0.66(1)}Ti_{0.355(7)}O_3$
PBZT10	$Pb_{0.90}Ba_{0.10}Zr_{0.65}Ti_{0.35}O_3$	$Pb_{0.89(1)}Ba_{0.097(2)}Zr_{0.657(8)}Ti_{0.352(4)}O_3$
PBZT20	$Pb_{0.80}Ba_{0.20}Zr_{0.65}Ti_{0.35}O_3$	$Pb_{0.79(1)}Ba_{0.194(4)}Zr_{0.66(1)}Ti_{0.351(6)}O_3$
PBZT30	$Pb_{0.70}Ba_{0.30}Zr_{0.65}Ti_{0.35}O_3$	$Pb_{0.684(8)}Ba_{0.294(5)}Zr_{0.659(7)}Ti_{0.352(4)}O_3$
PBZT40	$Pb_{0.60}Ba_{0.40}Zr_{0.65}Ti_{0.35}O_3$	$Pb_{0.58(2)}Ba_{0.39(1)}Zr_{0.66(2)}Ti_{0.36(3)}O_3$

The Ba-modified Pb(Zr, Ti)O_3 ceramic system (PBZT) has thus emerged as a promising ferroelectric system because of its rich variety of interesting physical properties of both technological and fundamental importance (Jonker *et al.*, 1980; Handerek *et al.*, 1999; Adamczyk *et al.*, 2001; Pan *et al.*, 2005).

Many years ago, a phase diagram as a function of barium content was proposed for the $(Pb_{1-x}Ba_x)(Zr_yTi_{1-y})O_3$ (PBZT) system (Ikeda, 1959). Since then, the dielectric properties of this system have been broadly investigated as a function of the Ba content (Jaffe *et al.*, 1971; Jonker *et al.*, 1980; Kanai *et al.*, 1994; Handerek *et al.*, 1999). Normal ferroelectric behavior and a rhombohedral structure has previously been observed in a $Pb_{1-x}Ba_xZr_{0.65}Ti_{0.35}O_3$ ceramic with $x < 0.40$ (Ikeda, 1959). However, the question as to which rhombohedral space group these compositions belong was not discussed. On the other hand, for $x > 0.40$ a cubic structure was observed (Ikeda, 1959). It has been recently observed that PBZT samples with $0.30 < x < 0.40$ present a ferroelectric relaxor behavior which could be explained by a less deformed octahedral environment of the Zr/Ti cations (Handerek *et al.*, 1999; Kanai *et al.*, 1994; Adamczyk *et al.*, 2001, 2006; Pan *et al.*, 2005; Adamczyk, 2006).

Structural information as a function of temperature has only been reported for $PbZr_{0.65}Ti_{0.35}O_3$. According to the PZT-proposed phase diagram (Jaffe *et al.*, 1971), at 300 K a phase transition from *R*3*m* to *R*3*c* is observed, while a phase transition from rhombohedral (*R*3*c*) to cubic is observed at 620 K.

In the present work, in order to obtain more detailed information about the structure of the PBZT system as a function of composition and temperature, Rietveld analysis of synchrotron X-ray powder diffraction data collected at different temperatures was undertaken for $Pb_{1-x}Ba_xZr_{0.65}Ti_{0.35}O_3$ ceramic samples with x = 0.00, 0.10, 0.20, 0.30 and 0.40. To the best of our knowledge, a structural determination using Rietveld analysis of X-ray or neutron diffraction data is not available for PBZT materials over a large range of Ba concentrations or even as a function of temperature.

2. Experimental

The samples studied, of nominal composition $Pb_{1-x}Ba_xZr_{0.65}Ti_{0.35}O_3$ with x = 0.00, 0.1, 0.2, 0.3 and 0.4 (abbreviated as PBZT*X* with *X* from 00 to 40) were prepared by the conventional mixed-oxides method. The precursors PbO, $BaCO_3$, ZrO_2 and TiO_2 were weighted according to each stoichiometry, and ball-milled in distilled water for 3 h. The slurry was dried and calcined in a covered alumina crucible at 1123 K for 3 h. Ceramic bodies were formed by uniaxial isostatic cold pressing and then fired at temperatures between 1523 and 1603 K for 3 h. The sintering occurred in closed Al_2O_3 crucibles at saturated PbO atmosphere and the highest density samples were chosen for the physical characterization.

The chemical compositions of PBZTX samples were determined by inductively coupled plasma atomic-emission spectrometry (ICP-AES, Varian model VISTA-MPX). HF (2 ml), HNO_3 (10 ml) and HCl (2 ml) were slowly added until 200 µg of each sample were consumed. The sample solution was then diluted with 90 ml of Mili-Q water. Table 1 shows a comparison between the nominal and experimental compositions where the oxygen contents were obtained by stoichiometric calculations. Scanning electron microscopy (SEM) revealed that the average grain-size of all fired samples was about 3–4 µm.

Low- and high-temperature X-ray diffraction (XRD) measurements were carried out at the Brazilian Synchrotron Light Laboratory (LNLS, D10B-XPD beamline). The XRD patterns were collected on a Huber diffractometer with θ–2θ geometry, λ = 1.3793 and/or 1.5292 Å. The instrument was calibrated using silicon (NIST SRM 640c). Each pattern consisted of 5000 steps, ranging from 20 to 120° in 2θ, with a step size of 0.02°. The count time was 0.5 s per step, from 20 to 90°, and 1.5 s per step, from 90 to 120°, and all patterns were normalized prior to refinement.

For investigations involving special thermal environments, a commercial closed-cycle He cryostat (Advanced Research Materials), with vibration damping and temperature control (10–450 K), and a homemade furnace (293–1273 K) were used. More details about the instrument can be seen in Ferreira *et al.* (2006). The geometry of the instrument did not enable rotation of the samples during data collection. To study the behavior of the phases with temperature, some peaks of each sample were selected and measured varying the temperature with a step of 10 K around the transition temperature. Several scans of the (104) and (110) peaks of PBZT10 and PBZT20, (211) of PBZT30 and (110) of PBZT40 were performed with λ = 1.3793 Å at different temperatures close to the possible phase-transition temperature. For the PBZT10 and PBZT20 samples, the data were collected with a step size of 0.01° with 0.5 s per step, and for the samples PBZT30 and PBZT40 the step was 0.02° with 0.5 s per step.

2.1. Structure refinement

Structural refinement was performed using the Rietveld method, as implemented in the computer program package *FULLPROF* (Rodríguez-Carvajal, 1990). A background polynomial was used with three coefficients for the PBZT00, PBZT10 and PBZT20 samples and four coefficients for PBZT20 at 630 K, and PBZT30. A cubic spline interpolation between a set of background points with refinable heights was used to model the background profile in the PBZT40 system, and the initial set with 72 background points was obtained

Table 2
Space group, temperature (K) and residuals obtained from Rietveld refinement for the $Pb_{1-x}Ba_xZr_{0.65}Ti_{0.35}O_3$ system.

The profile R_p, R_{wp} and R_{exp} are not corrected for background and the sum is extended to all points, according to the current CIF standard.

Sample	Space group	T	R_{Bragg}	R_f	R_p	R_{wp}	R_{exp}	R_{wp}/R_{exp}
PBZT00	*R*3*c*:*h*	300	17.0	11.8	18.6	23.8	13.0	1.83
	Pm$\bar{3}$*m*	650	17.6	11.4	16.8	21.1	12.03	1.75
PBZT10	*R*3*c*:*h*	300	10.8	8.41	13.7	17.9	12.3	1.45
	Pm$\bar{3}$*m*	750	11.8	8.91	13.2	17.1	13.4	1.27
PBZT20	*R*3*c*:*h*	300	12.9	8.72	15.7	20.3	14.63	1.39
	Pm$\bar{3}$*m*	630	15.1	11.9	14.1	18.1	12.95	1.39
PBZT30	*Pm*$\bar{3}$*m*	300	13.1	9.66	13.0	16.4	10.98	1.49
PBZT40	*Pm*$\bar{3}$*m*	300	10.6	5.4	8.81	11.4	3.99	2.86

† The $PZT_{(65/35)}$ cell parameter reported by Corker *et al.* (1998) (ICSD: 86136), used for comparison.

using *WinPLOTR* software (Roisnel & Rodríguez-Carvajal, 2000). Anisotropic strain broadening was modeled using a quartic form in reciprocal space. This interprets the strains as due to static fluctuations and correlations between metric parameters (Rodríguez-Carvajal *et al.*, 1991).

The standard material used for modeling the instrumental resolution was silicon, and the parameters of Straumanis & Aka (1952) were employed as an initial model for crystal structure refinement. The determined instrumental parameters (U_{ins}, V_{ins}, W_{ins}, X_{ins} and Y_{ins}) were used in the Rietveld refinement.

The PZT cell parameters with a Zr/Ti ratio of 65/35 given by the ICSD number 86136 (Corker *et al.*, 1998) were taken as an initial model for refinement and the Pb was fixed at the origin. Two space groups (*R*3*m* and *R*3*c*:*h*) were analyzed for the rhombohedral phase and the better result was obtained with *R*3*c*:*h*.

3. Results

Crystal data, data collection procedures and refinement results have been deposited.[1] The quality of the agreement between observed and calculated profiles in *FullProf* was measured by conventional factors, some of which are shown in Table 2 indicating relatively good refinements. Space groups are also shown in Table 2. To show the evolution of the deformation in the octahedra on increasing the quantity of Ba, the bond lengths and angles between the Ti—O atoms at 300 K are summarized in Table 3.

[1] Supplementary data for this paper are available from the IUCr electronic archives (Reference: KD5005). Services for accessing these data are described at the back of the journal.

A thermal hysteresis effect was observed on the transition temperature between the rhombohedral and cubic phases for the PBZT10 and PBZT20 samples. The measurements were carried out around the (110) peak of the cubic phase (see Figs. 1 and 2). When the temperature was increased, PBZT10 showed a phase transformation from rhombohedral to cubic between 523 and 543 K. However, when the temperature was decreased, the transformation from cubic to rhombohedral occurred between 513 and 503 K. PBZT20 showed the rhombohedral–cubic transformation between 453 and 463 K, and the cubic rhombohedral between 423 and 413 K, respectively.

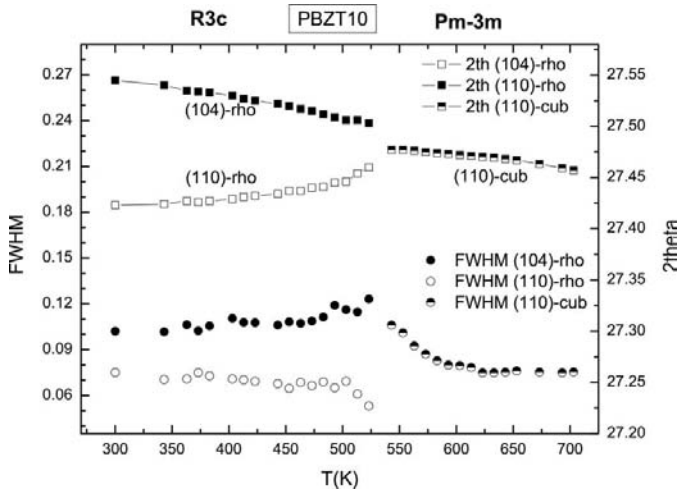

Figure 1
Temperature dependence of the FWHM (on the left) and position (on the right) of the (104) and (110) rhombohedral reflections, and (110) cubic reflection for the PBZT10 sample. The measurement was taken as the temperature increased.

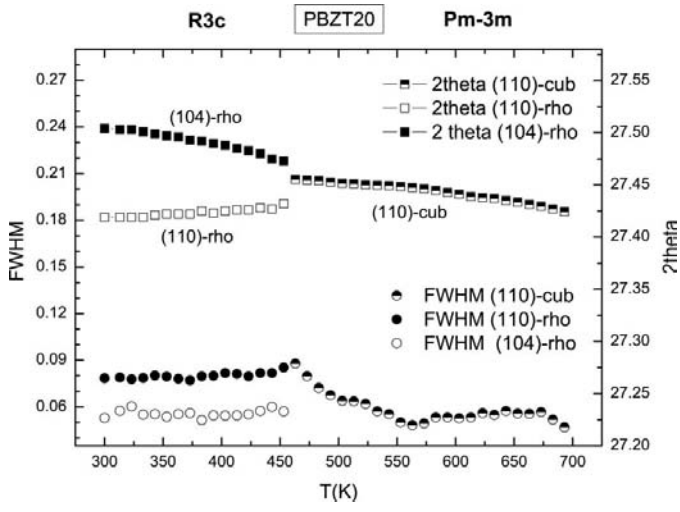

Figure 2
Temperature dependence of the FWHM (on the left) and position (on the right) of the (104) and (110) rhombohedral reflections, and (110) cubic reflection for the PBZT20 sample. The measurement was taken as the temperature increased.

Table 3
Bond lengths (Å) and angles (°) involving the Ti and O atoms at 300 K.

The superscript number indicates the symmetry transformations used to generate equivalent atoms.

Sample	Bond		Angle	
PBZT00	3TiO*a*^{i}	1.87 (2)	O*a*—Ti—O*a*	104.9 (8)
	3TiO*b*^{ii}	2.30 (3)	O*b*—Ti—O*b*	75.4 (1)
			O*a*—Ti—O*b*	87.7 (1)
				87.8 (1)
				158.6 (1)
PBZT10	3TiO*a*^{i}	1.97 (2)	O*a*—Ti—O*a*	99.6 (1)
	3TiO*b*^{ii}	2.17 (2)	O*b*—Ti—O*b*	80.1 (9)
			O*a*—Ti—O*b*	89.1 (1)
				89.4 (1)
				166.1 (1)
PBZT20	3TiO*a*^{i}	2.05 (2)	O*a*—Ti—O*a*	99.8 (1)
	3TiO*b*^{ii}	2.10 (2)	O*b*—Ti—O*b*	79.4 (1)
			O*a*—Ti—O*b*	89.1 (2)
				89.9 (2)
				165.5 (2)
PBZT30	6TiO^{iii}	2.056214 (1)	O—Ti—O	90
				180
PBZT40	6TiO^{iii}	2.058016 (2)	O—Ti—O	90
				180

Symmetry transformations used to generate equivalent atoms: (i) x, y, z; $-x+y, -x, z$; $-y, x-y, z$; (ii) $-\frac{1}{3}+x, \frac{1}{3}+x-y, -\frac{1}{6}+z$; $\frac{2}{3}-y, \frac{1}{3}-x, -\frac{1}{6}+z$; $-\frac{1}{3}-x+y, -\frac{2}{3}+y, -\frac{1}{6}+z$; (3) x, y, z; $z, y, 1-x$; $x, 1-z, y$; $x, -z, y$; $x, y, 1+z$; $1+z, y, 1-x$.

4. Discussion

The results obtained for PBZT00 are very similar to those reported for PZT(65/35) samples (Corker *et al.*, 1998), the difference being that here the atomic positions of the Zr and Ti cations converged to the same value. In Fig. 3 the cell parameters of the *R*3*c*:*h* phase were given as *R*3*c*:*r* to clearly show the evolution of the rhombohedral phase upon increasing the Ba content. When Ba content is increased from $x = 0.00$ to 0.20, the angle α increases, approaching the value of 60° which is characteristic of the cubic structure. When the amount of Ba is increased, the distances between the Ti—O atoms (Ti—O*a* and Ti—O*b* pairs) at room temperature (see Table 3) change until they become equal for the PBZT30 and PBZT40 samples, which present a cubic phase with a regular TiO_6 octahedra. Our results are in good agreement with the structural model proposed (Ikeda, 1959) for the PBZT10 and PBZT20 samples which were indexed as rhombohedral structures. However, both PBZT30 and PBZT40 samples, that according to the work of Ikeda (1959) should also be rhombohedral, from our XRD data refinement present a cubic structure. These results are in good agreement with the dielectric measurements conducted on the PBZT30 and PBZT40 samples that show a relaxor behavior for which a less deformed octahedral structure should be expected (Mastelaro *et al.*, 2006; Pan *et al.*, 2005).

As can be seen in Figs. 1 and 4 the full width at half-maximum (FWHM) of the (110) rhombohedral reflection of PBZT10 decreases with an increase in temperature. Also the separation between the 2θ angles from (104) and (110) rhombohedral reflections decreases with increasing temperature, collapsing into the (110) cubic reflection at 543 K. This temperature may be considered to reproduce well the ferroelectric paraelectric phase transition temperature at T_c = 552 K as determined from the temperature dependence of the relative dielectric permitivity (Mastelaro *et al.*, 2006). On raising the temperature to 703 K, the (110) peak moves slightly towards smaller 2θ values, reflecting the increase in the cell parameter with temperature (Fig. 5). Fig. 2 shows the similar behavior of PBZT20; the phase transition occurs at 463 K, which is comparable with the ferroelectric paraelectric phase-transition temperature of T_c = 480 K, determined from dielectric measurements. Compared with undoped PZT the temperature of the phase transition decreases. On the other hand (Figs. 5 and 6), the PBZT30 and PBZT40 samples did not

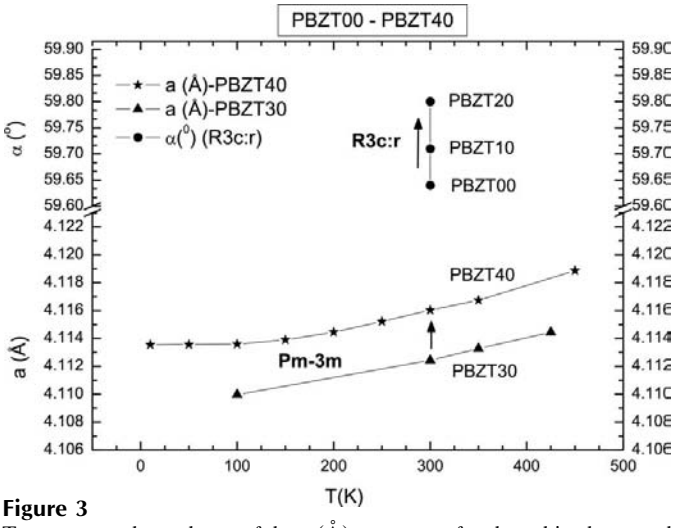

Figure 3
Temperature dependence of the *a* (Å) parameter for the cubic phase, and the α angle (°) for the rhombohedral phase (*R*3*c*:*r*) obtained from the Rietveld refinement. The arrow indicates the direction in which the Ba content is increased.

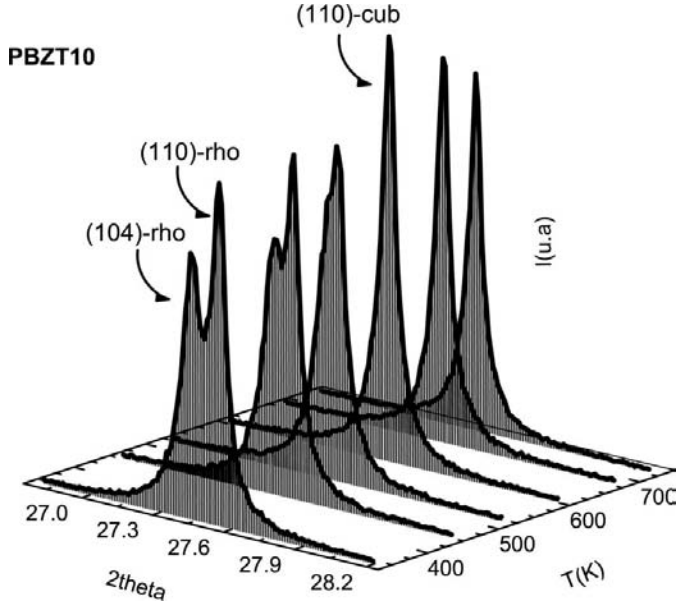

Figure 4
Evolution of the (104) and (110) reflections from the temperature increase for the PBZT10 sample.

show any phase transformation in the temperature interval from 10 to 450 K. Thus, as expected for a relaxor ferroelectric (Samara, 2005; de Mathan *et al.*, 1991), these results show that there is no macroscopic phase transition in the PBZT30 and PBZT40 samples in the temperature range where dielectric permitivity peaks are observed.

In all samples the cubic phase shows an increase in the cell parameter with an increase in Ba content (see Fig. 5), as expected, due to the fact that the ionic radius ($r_{Ba^{2+}}$ = 1.34 Å) is greater than the Pb ionic radius ($r_{Pb^{2+}}$ = 1.21 Å). Moreover, it is seen that with increasing temperature, the cell parameter of the cubic phases also increases as a result of thermal expansion.

When the Ba content is increased from x = 0.10 to 0.20 in the PBZT ceramics, the transition temperature from the rhombohedral to the cubic phases decreases (Figs. 1 and 2) in good agreement with electrical measurements (Mastelaro *et al.*, 2006; Ikeda, 1959). As shown in §3, these samples exhibit a hysteresis effect around the phase transition, similar to the result observed in the barium titanate ceramic (Jaffe *et al.*, 1971).

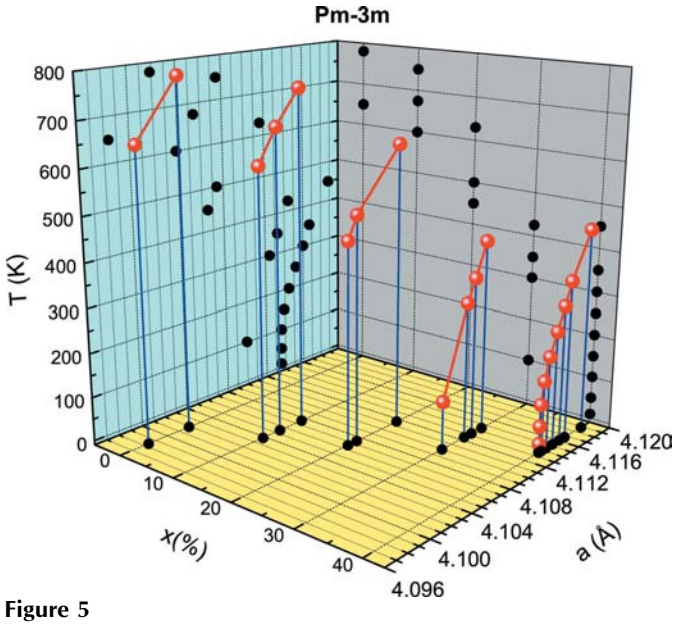

Figure 5
Cell parameter (a) dependence of the Ba content (x) and temperature (T) in the $Pb_{1-x}Ba_xZr_{0.65}Ti_{0.35}O_3$ system for the cubic phase. The red points are obtained from the Rietveld refinement and the black are the projections in the corresponding plane.

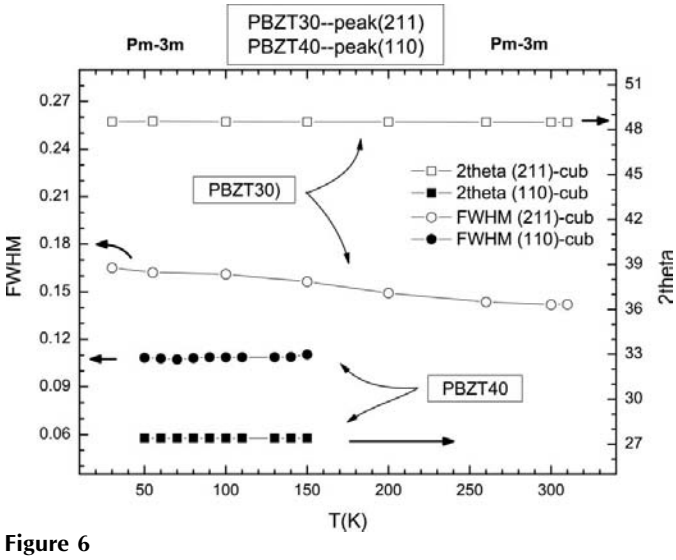

Figure 6
Temperature dependence of the FWHM (on the left) and position (on the right) of the (211) cubic reflection for the PBZT30 sample and (110) for the PBZT40 samples.

5. Conclusions

The effect of the addition of barium oxide on the structure of PZT samples was evaluated. When the Ba content is increased from x = 0.10 (PBZT10) to x = 0.20 (PBZT20), the phase transition from rhombohedral to cubic was observed to be shifted to lower temperatures (543 and 463 K, respectively) when compared with the undoped PZT ceramic (630 K). This phase transition presents thermal hysteresis for both samples, typical of many materials. The samples with x = 0.30 (PBZT30) and 0.40 (PBZT40) were both cubic. The results also confirm the qualitative analysis of the XRD data found in the literature for PBZT10 and PBZT20. On the other hand, both PBZT30 and PBZT40 remained cubic within the entire temperature range analyzed. Our results are in good agreement with the dielectric behavior observed for both samples.

The authors are grateful to FAPESP and CNPq for financial support. This research was partially carried out at the Brazilian Synchrotron Light Laboratory (LNLS).

References

Adamczyk, M. (2006). *Ceram. Int.* **32**, 923–928.
Adamczyk, M., Ujma, Z. & Handerek, J. (2001). *J. Appl. Phys.* **89**, 542–547.
Adamczyk, M., Ujma, Z., Szymczak, L. & Soszynski, A. (2006). *Ceram. Int.* **32**, 877–881.
Corker, D. L., Glazer, A. M., Whatmore, R. W., Stallard, A. & Faut, F. (1998). *J. Phys. Condens. Matter*, **10**, 6251–6269.
Ferreira, F. F., Granado, E., Carvalho Jr, W., Kycia, S. W., Bruno, D. & Droppa Jr, R. (2006). *J. Synchrotron Rad.* **13**, 46–53.
Frantti, J., Ivanov, S., Eriksson, S., Rundlof, H., Lantto, V., Lappalainen, J. & Kakihana, M. (2002). *Phys. Rev. B*, **66**, 064108/1–15.
Handerek, J., Adamczyk, M. & Ujma, Z. (1999). *Ferroelectrics*, **233**, 253–270.
Ikeda, T. (1959). *J. Phys. Soc. Jpn*, **14**, 168–174.
Jaffe, B., Cook, W. R. & Jaffe, H. (1971). *Piezoelectric Ceramics.* London, New York: Academic Press.
Jonker, G. H., Juarez, R., Burggraf, A. J. & Stenger, C. G. F. (1980). *Ferroelectrics*, **24**, 293–296.
Joseph, J., Vimala, T., Sivasubramanian, V. & Murthy, V. (2000). *J. Mater. Sci.* **35**, 1571–1575.
Kanai, H., Furukawa, O., Abe, H. & Yamashita, Y. (1994). *J. Am. Ceram. Soc.* **77**, 2620–2624.
Kozielski, L., Adamczyk, M., Lisinska-Czekaj, A., Orkisz, T., Piechowiak, M. & Czekaj, D. (2006). *Phase Transitions*, **79**, 427–433.

Lines, M. & Glass, A. (2001). *Principles and Applications of Ferroelectrics and Related Materials.* Oxford: Clarendon Press; New York: Oxford University Press.
Mastelaro, V. R., Doriguetto, A. C., Neves, P. P., Garcia, D., Lente, M. H., Mascarenhas, Y. P., Michalowicz, A. & Eiras, J. A. (2006). *Ferroelectrics*, **339**, 219–226.
Mathan, N. de, Husson, E., Calvarin, G., Gavarri, J. R., Hewat, A. W. & Morel, A. (1991). *J. Phys. Condens. Matter*, **3**, 8159–8171.
Noheda, B., Cox, D., Shirane, G., Gonzalo, J., Cross, L. & Park, S. (1999). *Appl. Phys. Lett.* **74**, 2059–2061.
Pan, M., Rayne, R. & Bender, B. (2005). *J. Electroceram.* **14**, 139–148.
Ragini, Ranjan, R., Mishra, S. & Pandey, D. (2002). *J. Appl. Phys.* **92**, 3266–3274.
Rodríguez-Carvajal, J. (1990). *Abstracts of Satellite Meeting on Powder Diffraction of the XV Congress of the IUCr*, June 2005, Toulouse, France, p. 127.
Rodríguez-Carvajal, J., Fernandez-Diaz, M. T. & Martinez, J. L. (1991). *J. Phys. Condens. Matter*, **3**, 3215–3234.
Roisnel, T. & Rodríguez-Carvajal, J. (2000). *Materials Science Forum, Proceedings of the Seventh European Powder Diffraction Conference* (EPDIC 7), edited by E. R. Delhez & E. J. Mittenmeijer, pp. 118–123. Trans Tech Publications.
Samara, G. A. (2005). *Phys. Rev. B*, **71**, 224108.
Straumanis, M. E. & Aka, E. Z. (1952). *J. Appl. Phys.* **23**, 330–334.
Woodward, D., Knudsen, J. & Reaney, I. M. (2005). *Phys. Rev. B*, **72**, 104110/1–8.